Mini Review

Recent advances in synthesis and structural diversity of tin oxo clusters

Ni Zhen, Fang-Fang Liu, Zuo-Hu Zhou, Lei Zhang*

Institute of Modern Optics, Tianjin Key Laboratory of Micro-scale Optical Information Science and Technology, College of Electronic Information and Optical Engineering, Nankai University, Tianjin 300350, China.

***Correspondence to:** Prof. Lei Zhang, Institute of Modern Optics, Tianjin Key Laboratory of Micro-scale Optical Information Science and Technology, College of Electronic Information and Optical Engineering, Nankai University, Tianjin 300350, China. E-mail: zhanglei3915@nankai.edu.cn

ORCID: Lei Zhang (0000-0001-7720-4667)

How to cite this article: Zhen N, Liu FF, Zhou ZH, Zhang L. Recent advances in synthesis and structural diversity of tin oxo clusters. *Chem Synth* 2026;6:[Accept]. http://dx.doi.org/10.20517/cs.2025.108

Received: 26 November 2025 | **Revised:** 16 January 2026 | **Accepted:** 29 January 2026

Abstract

Tin oxo clusters (TOCs) are a distinctive class of metal oxo clusters (MOCs) that serve as a unique bridge between molecular design and macroscopic material properties. This review provides a comprehensive and systematic overview of recent advances in the synthesis, structural diversity, and functional applications of TOCs. We elaborate on how innovative synthetic strategies - including solvothermal synthesis, ligand-directed assembly, and heterometallic incorporation with secondary metal ions - enable exquisite control over the nuclearity, architectural topology, and surface chemistry of TOCs. The discussion explores the rich structure of TOCs, spanning from fundamental cage-like and drum-shaped architectures to elaborate high-nuclearity macrocycles and hybrid frameworks, all unified by well-defined Sn–O–Sn core motifs that afford atomic-level

insights into tin oxide coordination chemistry. Furthermore, this review offers a forward-looking perspective by identifying critical future research directions, including the development of predictive synthesis methodologies, multifunctional integration *via* structural engineering, and translational research toward practical applications.

Keywords: Tin oxo clusters, metal oxo clusters, cluster chemistry, synthetic chemistry, heterometallic compounds

INTRODUCTION

Metal oxo clusters (MOCs) are discrete polynuclear assemblies that serve as architectural bridges between simple molecular complexes and extended solid-state materials[1-5]. These nanoscale clusters have attracted sustained research interest over recent decades due to their structural diversity and promising applications in catalysis[6-8], energy storage[9,10], nanopatterning[11-15], and biomedicine[16-19]. Characteristically, MOCs exhibit well-defined atomic arrangements consisting of metal cations interconnected by μ_2- or μ_3-oxo bridges, stabilized and functionalized by peripheral organic ligands [**Figure 1**][20]. Their tunable nuclearity and versatile surface chemistry allow MOCs to merge the stability and electronic properties of inorganic oxides with the synthetic precision and processability of molecular species, making them ideal platforms for probing structure-property relationships and developing advanced functional materials. Based on metal composition, MOCs are broadly divided into two categories. The first encompasses transition metal oxo clusters, which include early transition metals (e.g., V, Mo, W, Nb, Ta)[21-23], lanthanides (Ln)[24], and other key transition metals (e.g., Ti, Zr, Mn, Fe, Co, Ni, Cu, Zn)[25-27]. This category is exemplified by polyoxometalates (POMs), well-known for their rich redox chemistry and catalytic applications. The second category comprises main-group metal oxo clusters, formed by elements such as Al[28], In[29], Sn[30], and Bi[31], which have gained increasing attention due to their diverse structural topologies and distinctive physicochemical properties arising from highly ionic bonding and flexible coordination geometries.

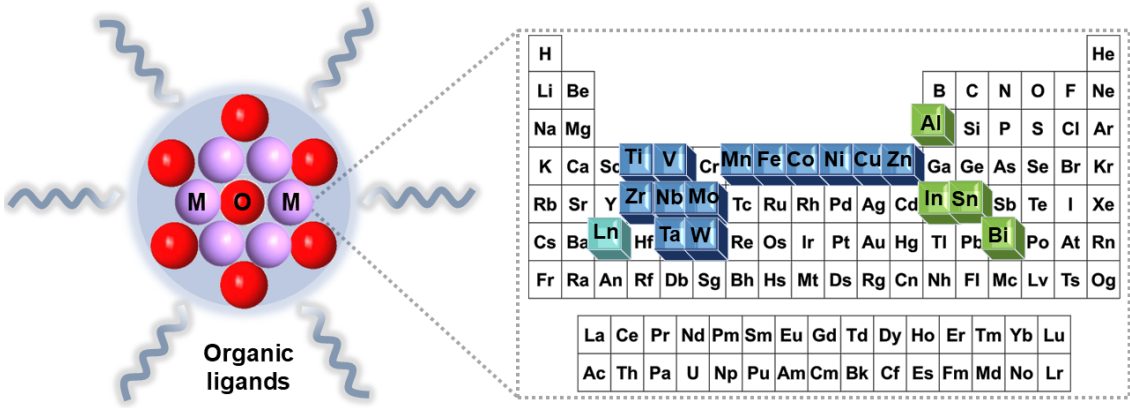

Figure 1. Structural and elemental composition of MOCs. Left: Atomic-precise structure of MOCs, featuring a metal-oxo core and a tunable organic ligand shell. Right: An expanded view highlighting the key metallic elements that constitute MOCs. This schematic was created by the authors.

Among main-group MOCs, tin oxo clusters (TOCs) constitute a structurally distinctive class that effectively bridges molecular design and macroscopic material properties[32]. Their architecture features well-defined {Sn_xO_y} cores built from oxo-bridged Sn–O–Sn linkages, strategically encapsulated and functionalized by organic ligands such as carboxylates[33], phosphonates[34], and alkoxides[35]. The precise molecular design and high crystallinity of TOCs facilitate atomic-resolution structural characterization *via* X-ray diffraction, offering unprecedented insights into bonding, topology, and ligand–core interactions. These details often obscured in conventional tin oxides by structural heterogeneity and compositional complexity. Structurally, TOCs exhibit remarkable diversity, ranging from simple cage-like units, such as tetranuclear cubes and ladders, to complex high-nuclearity architectures including wheels and macrocycles. The structural versatility stems from the flexible coordination geometry of tin and its propensity to form stable oxo-bridged motifs under controlled synthesis.

As an important and dynamically evolving branch of cluster chemistry, research on the synthesis of TOCs has witnessed remarkable progress over recent decades, driven by the growing demand for high-performance materials in nanolithography[36-40], catalysis[41], and optoelectronics[42,43]. It is worth mentioning that in the context of high-resolution lithography applications, particularly for next-generation extreme ultraviolet (EUV) lithography, tin has garnered significant attention due to its inherently high EUV absorption cross-section[44-46]. This intrinsic property makes tin-based materials highly

efficient photoresists capable of achieving exceptional patterning sensitivity and resolution at lower radiation doses. Continuous exploration into synthetic methodologies, from traditional solution-based routes to advanced solventothermal and solid-state strategies, has led to the preparation of an ever-expanding range of novel TOC structures, with developments progressively advancing toward higher nuclearity (from 4-core to 34-core clusters), multidimensional architectures (0D cages, 1D rods, 2D layers, 3D frameworks), mixed-ligand coordination, and hybrid functionalization[30]. Based on the presence or absence of Sn–C bonds, TOCs can be broadly categorized into two types, each with distinct synthetic logic and application potential: (i) organic TOCs feature stable Sn–C bonds (e.g., Sn–butyl, Sn–phenyl) and are typically synthesized from organotin precursors such as butylstannonic acid (n-BuSn(O)OH), dibutyltin dichloride ($n\text{-}Bu_2SnCl_2$), or triphenyltin chloride (Ph_3SnCl), where the Sn–C bond acts as a structural anchor guiding the assembly of well-defined frameworks while enabling post-synthetic modification *via* ligand functionalization; (ii) Inorganic (non-alkyl) TOCs lack Sn–C bonds and are generally prepared from inorganic tin salts like $SnCl_4$, $SnCl_2$, SnF_2, or $SnSO_4$, with their synthesis focusing on regulating hydrolysis kinetics to avoid amorphous oxide precipitation.

This review provides a systematic overview of recent advances in the synthesis, structural diversity, and functional applications of TOCs. We detail innovative synthetic strategies, including solvothermal synthesis, ligand-directed assembly, coordination-delayed hydrolysis strategy, and heterometallic strategy, that facilitate precise control over nuclearity, architecture, and functionality. The presented structures are systematically categorized into organotin oxo clusters, non-alkyl tin oxo clusters, and heterometallic tin oxo clusters, tracing the architectural evolution from foundational cages to high-nuclearity wheels and macrocycles. Furthermore, the review critically examines their performance in key application areas, such as high-resolution lithography, electrocatalysis, and third-order nonlinear optics (NLO).

Organotin Oxo Clusters

The structural diversity and nuclearity control of organotin oxo clusters are tightly regulated by the rational design of organic substituents (predominantly carboxylic acids, phosphinic acids, borate ligands, and selenite ligands) and reaction conditions (e.g.,

solvent polarity, protic/aprotic nature, and stoichiometry) [**Table 1**]. Modulating these factors enables the precise construction of specific structural motifs, laying the foundation for exploring structure-property relationships in functional materials. Organotin oxo clusters has been significantly advanced through the discovery and characterization of several classic topologies [**Figure 2**]. The cubic cluster [n-$BuSn(O)O_2CR]_4$ is a tetranuclear (Sn_4) structure with a cubic $\{Sn_4O_4\}$ core, where each Sn center is coordinated by one butyl group (Sn–C) and two carboxylate ligands ($–O_2CR$), favored when using short-chain, low-steric-hindrance phosphinic acids (di-tert-butylphosphinic acid, di-benzylphosphinic acid) and non-polar solvents (benzene, toluene)[47,48]; The classic planar Sn_4 cluster (e.g., $[(n\text{-}Bu_2Sn)_2(\mu_3\text{-}O)(\mu\text{-}OH)L]_2$) features a tetranuclear framework with two $\{Sn_2(\mu\text{-}O)\}$ units bridged by carboxylate ligands, forming a "ladder" structure where Sn centers alternate along the "rungs" and μ-O bridges act as the "side rails", stabilized by symmetric carboxylates[49,50]; The ladder-shaped cluster $[(n\text{-}BuSn(O)O_2CR)_2\text{-}n\text{-}BuSn(O_2CR')_3]_2$ is a hexanuclear (Sn_6) structure resembling a "ladder", with alternating Sn_3 units linked by carboxylate bridges, and the asymmetric distribution of carboxylate ligands ($–O_2CR$ and $–O_2CR'$) introduces structural flexibility useful for supramolecular assembly[51]; The hexameric drum-type structure $[R'SnO(O_2CR)]_6$ is a cylindrical (Sn_6) framework with a central $\{Sn_6O_6\}$ core, where six Sn centers form the "drum body". This type of structures is typically obtained *via* 1:1 reaction of [n-BuSn(O)OH] with carboxylic acids. The chelating carboxylates capping the top and bottom of the cylindrical core and enhance the thermal stability of the clusters [52]. Football-like $[(RSn)_{12}O_{14}(OH)_6]^{2+}$ (Sn_{12}) clusters represent a class of ligand-free TOCs, where each Sn center is coordinated by one alkyl group (R). The formation of Sn_{12} is often driven by solvent polarity. For example, polar protic solvent water or aprotic 1,2-dimethoxyethane promotes the aggregation of Sn centers into the $\{Sn_{12}O_{14}(OH)_6\}$ spherical core *via* oxo/hydroxo bridging, rendering it highly soluble in polar solvents and suitable for thin-film fabrication[53,54]; As well as Keggin-type organotin oxo clusters are derived from the classic Keggin anion structure ($[XM_{12}O_{40}]^{n-}$), replacing transition metals (M) with organotin units (e.g., $n\text{-}BuSn^{3+}$) and incorporating central cations ($X = Na^+, Ca^{2+}$), exhibiting unique isomerism (α, β, γ) and stabilized by electrostatic interactions with counterions[55-57].

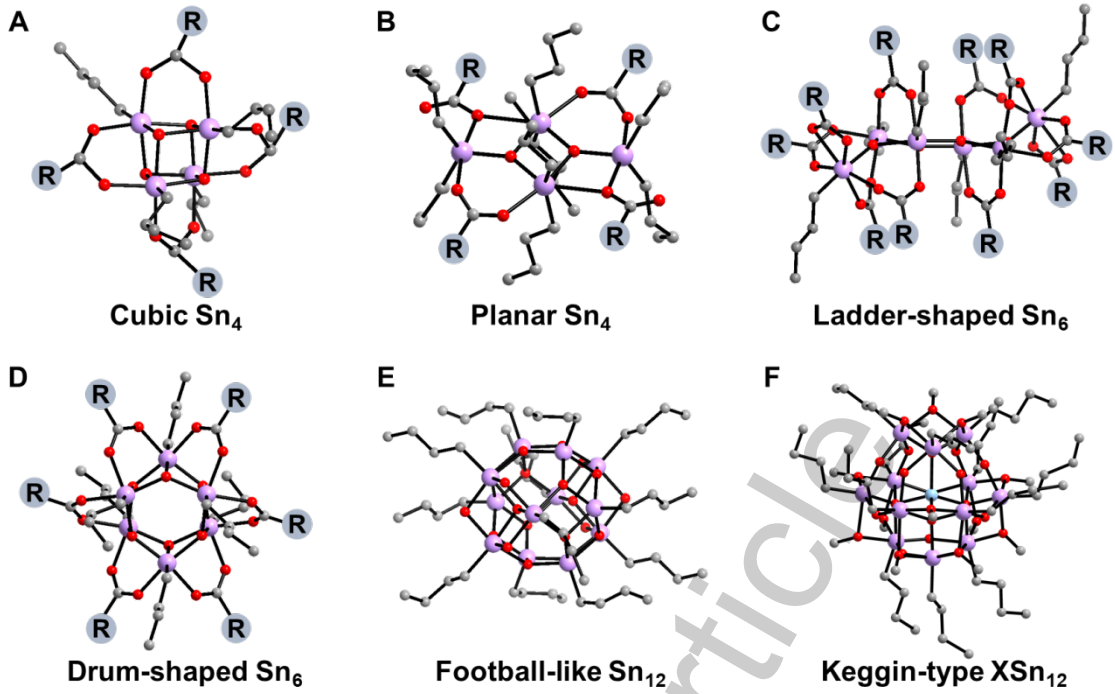

Figure 2. Examples of foundational organotin oxo cluster architectures: (A) cubic Sn_4[47], (B) planar Sn_4[49], (C) ladder-shaped Sn_6[51], (D) drum-shaped Sn_6[52], (E) football-like Sn_{12}[54], and (F) Keggin-type XSn_{12}[55]. Color code: Sn, purple; O, red; C, grey; X, light blue. The crystal structures were redrawn based on crystallographic data from literatures.

Table 1. Summary of topology, nuclearity, formula, ligands, reaction solvent for organotin oxo clusters

Topology and nuclearity	Formula	Ligands	Reaction solvent	Ref.
Cubic Sn_4	[n-BuSn(O)O_2P(t-Bu)$_2$]$_4$	di-tert-butylphosphinic acid	benzene	[47]
Cubic Sn_4	[n-BuSn(O)O_2P(CH_2Ph)$_2$]$_4$	di-benzylphosphinic acid	toluene	[47]
Cubic Sn_4	[n-BuSn(O)O_2P(C_6H_{11})$_2$]$_4$	dicyclohexyl phosphinic acid	toluene	[48]

Planar Sn_4	$\{[n\text{-}Bu_2Sn(O_2CC_9H_9N_2)]_2O\}_2$	2-benzimidazolepropionic acid	toluene and ethanol	[49]
Planar Sn_4	$[(n\text{-}Bu_2Sn)_2(\mu_3\text{-}O)(\mu\text{-}OH)L]_2$	2-chloroisonicotinic acid	methanol	[50]
Ladder-shaped Sn_6	$[(n\text{-}BuSn(O)O_2CPh)_2\text{-}n\text{-}BuSn(O_2CPh)_3]_2$	benzoic acid	dichloro methane	[51]
Drum-shaped Sn_6	$[n\text{-}BuSn(O)O_2CC_6H_4NO_2]_6\cdot 3C_6H_6$	nitrobenzoic acid	dichloro methane	[51]
Drum-shaped Sn_6	$[n\text{-}BuSn(O)O_2CC_5H_9]_6\cdot C_6H_6$	cyclopentane-carboxylic acid	benzene	[52]
Football-like Sn_{12}	$[(n\text{-}BuSn)_{12}O_{14}(OH)_6]Cl_2\cdot 2H_2O$	-	Water	[53]
Football-like Sn_{12}	$[(n\text{-}BuSn)_{12}O_{14}(OH)_6](OH)_2$	-	1,2-dimethoxyethane	[54]
Keggin-type $CaSn_{12}$	$[CaO_4(n\text{-}BuSn)_{12}(O)_4(OH)_8(OCH_3)_{12}]\cdot 2[OH]$	-	methanol	[55]
Keggin-type $NaSn_{13}$	$[NaO_4(n\text{-}BuSn)_{12}(OH)_3(O)_9(OCH_3)_{12}(Sn(H_2O)_2)]$	-	methanol	[56]
Keggin-type $NaSn_{12}$	$[NaO_4(n\text{-}BuSn)_{12}(O)_5(OCH_3)_{12}(OH)_7]$	-	methanol	[57]
Rod-like Sn_{26}	$[(n\text{-}BuSn)_{22}Sn_4(OH)_{26}O_{22}(TZAC)_6]\cdot 4Cl\cdot 2(TZAC)\cdot 2(CH_3OH)\cdot 8H_2O$	1H-tetrazole-1-acetic acid	methanol, isopropa-nol and water	[58]
Rod-like Sn_{26}	$[(n\text{-}BuSn)_{22}Sn_4(OH)_{26}O_{22}(IANO)_6]\cdot 6(IANO)\cdot 6(CH_3OH)\cdot 4H_2O$	isonicotinic acid N-oxide	methanol, isopropa-	[58]

Rod-like Sn_{26}	$[(n\text{-}BuSn)_{22}Sn_4(OH)_{26}O_{22}(IANO)_6]$ $[(n\text{-}BuSn)_2(OH)_2(IANO)Cl_4]_2 \cdot 4Cl \cdot 6CH_3OH \cdot 10H_2O$	isonicotinic acid N-oxide	methanol, isopropanol and water	[58]
Cage-type Sn_{34}	$[(n\text{-}BuSn)_{34}Na_2(OH)_{14}O_{40}(PA)_8] \cdot 2(PA) \cdot 8H_2O$	2-picolinic acid	acetonitrile	[58]
Macrocyclic Sn_8	$[(n\text{-}BuSn)_8(SeO_3)_{16}]$	-	dimethyl sulfoxide and methylamine	[59]
Macrocyclic Sn_{12}	$[(n\text{-}BuSn)_{12}(\mu_2\text{-}O)_4(\mu_3\text{-}O)_{12}(SeO_3)_8]$	-	3,5-dimethylpiperidine and water	[59]
Macrocyclic Sn_{12}	$[(n\text{-}BuSn)_{12}(ClO_4)(\mu_3\text{-}O)_{12}(SeO_3)_8]$	-	4-methylpiperidine and water	[59]
Macrocyclic $Sn_{12}Fe_8$	$[(n\text{-}BuSn)_{12}Fe_{18}(\mu_4O)_6(C_2H_4O_2)_{24}(SeO_3)_{18}]$	-	N,N,N,N,N-pentamethyldiethylenetriamine and	[59]

	ethylene glycol (EG)

Between 2018 and 2020, Nyman et al. made significant contributions to alkyltin Keggin synthesis, reporting a series of Keggin ions: β-[NaO_4(n-BuSn)$_{12}$ $(OH)_3(O)_9(OCH_3)_{12}(Sn(H_2O)_2)$] (β-$NaSn_{13}$), [$NaO_4$(n-BuSn)$_{12}(O)_5(OCH_3)_{12}(OH)_7$] (β- and γ-$NaSn_{12}$), γ-[$NaO_4$(n-BuSn)$_{12}(OH)_6(O)_7(OCH_3)_{11}$(n-BuSn$OCH_3$)] (γ-$NaSn_{13}$) and β-[$CaO_4$(n-BuSn)$_{12}(O)_4(OH)_8(OCH_3)_{12}$]·2[OH] (β-$CaSn_{12}$), all derived from butyltin precursors[55-57]. The Keggin ions share a core framework of four {Sn_3O_4} trimers surrounding a central tetrahedral cation (Na^+ or Ca^{2+}), but differ in isomerism and capping: β-$NaSn_{12}$ adopts C_{3v} symmetry with all trimers linked by corner-sharing; γ-$NaSn_{12}$ has C_{2v} symmetry with one edge-sharing and five corner-sharing trimer connections; β/γ-$NaSn_{13}$ are capped with an additional Sn center (five-coordinate SnO_4C for γ-$NaSn_{13}$, $Sn(H_2O)_2$ for β-$NaSn_{13}$). β-$CaSn_{12}$ represents the first example of a four-coordinate Ca^{2+} (average Ca-O bond length: 2.28 Å) in an inorganic structure and demonstrates that the size and charge of the central cation significantly influence the overall stability and isomerization behavior of tin Keggin clusters. Typically, the Na-centered clusters can be obtained *via* a one-step reaction of n-$BuSnCl_3$ with NaOH in methanol (1:4 Sn:OH ratio), yielding colorless crystals within 24 hours. In contrast, β-$CaSn_{12}$ required solvothermal conditions (100 °C for 24 hours) with solid $Ca(OH)_2$ as the central cation source. These clusters feature methoxy (OCH_3^-) and hydroxo (OH^-) bridging ligands derived from methanol hydrolysis, with Sn-bound butyl groups imparting organic solubility. Additionally, their studies revealed that β-$NaSn_{12}$ is the most stable isomer - unlike most Keggin systems favoring high-symmetry α-configurations [**Figure 3**]. The butyltin Keggin system uniquely prefers the low-symmetry β-configuration driven by steric repulsion between butyl groups. This provides crucial insights into the study of low-symmetry Keggin isomers and the factors controlling isomer selectivity and stability.

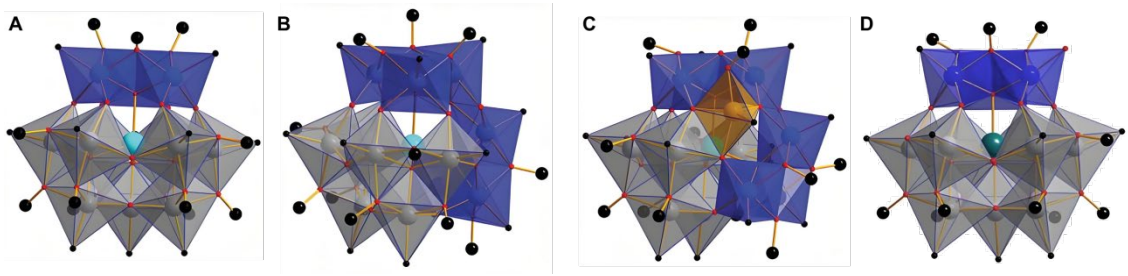

Figure 3. (A-C) Crystal structures of β-$NaSn_{12}$, γ-$NaSn_{12}$, γ-$NaSn_{13}$, respectively[57]. Copyright 2018, Royal Society of Chemistry. (D) Crystal structures of β-$CaSn_{12}$[55]. Copyright 2020, American Chemical Society. Color code: Sn, gray and blue polyhedra; Na, light blue; Ca, teal; O, red; C, black.

In recent years, synthetic efforts have further diversified the structural landscape of organotin-oxo clusters, yielding novel high-nuclearity architectures that push the limits of cluster assembly. The structural evolution of organotin-oxo clusters is governed by the dynamic interplay between precursor reactivity and synthetic conditions, including ligand design, solvent environment, and temperature. In 2019, Zhang et al. achieved the synthesis of higher-nuclearity TOCs, including three rod-like Sn_{26} clusters with different ligands ($[(n\text{-}BuSn)_{22}Sn_4(OH)_{26}O_{22}(TZAC)_6]\cdot 4Cl\cdot 2(TZAC)\cdot 2CH_3OH\cdot 8H_2O$ (HTZAC = 1*H*-tetrazole-1-acetic acid), $[(n\text{-}BuSn)_{22}Sn_4(OH)_{26}O_{22}(IANO)_6]\cdot 6(IANO)\cdot 6CH_3OH\cdot 4H_2O$, and $[(n\text{-}BuSn)_{22}Sn_4(OH)_{26}O_{22}(IANO)_6][(n\text{-}BuSn)_2(OH)_2(IANO)Cl_4]_2\cdot 4Cl\cdot 6CH_3OH\cdot 10H_2O$ (HIANO = isonicotinic acid N-oxide)) and the cage-type dimeric $[(n\text{-}BuSn)_{34}Na_2(OH)_{14}O_{40}(PA)_8]\cdot 2(PA)\cdot 8H_2O$ (Sn_{34}, HPA = 2-picolinic acid). The Sn_{26} clusters feature a novel layered nanorod architecture (core size: 1.6×1.0 nm) composed of five tin-oxo layers: two planar {Sn_5} units, two capped {Sn_7} moieties, and one central {Sn_2} dimer [**Figure 4**]. The {Sn_7} and {Sn_5} units are linked *via* five μ3-O atoms to form {Sn_{12}} moieties, which are further bridged by the central {Sn_2} dimer to construct the Sn_{26} core, with peripheral TZAC or IANO ligands stabilizing the structure. This layered topology is reminiscent of the tin-oxo layers in rutile SnO_2, making Sn_{26} an ideal molecular model for SnO_2 materials. The Sn_{34} cluster (core size: 2.6×1.1 nm) adopts a unique cage-dimer structure, assembled from two asymmetric {Sn_{12}} and {Sn_{22}} cages linked by Na atoms and PA ligands; the {Sn_{22}} cage consists of a top {Sn_3} moiety, two middle {Sn_6} circles, and a bottom {Sn_7} base, encapsulating a central Na^+ *via* six oxygen atoms. The Sn_{26} clusters were obtained in a mixed protic solvent system of methanol/isopropanol/water, while the Sn_{34} cluster was successfully synthesized by

switching to the aprotic solvent acetonitrile (CH_3CN) to modulate the configuration of Sn–O building units and their connection modes [**Table 1**]. Additionally, the introduction of $SnCl_4$ as a co-precursor enhanced tin availability and significantly improved the yield of the Sn_{26} cluster. Notably, the Sn_{34} cluster remains the highest nuclearity TOC reported to date, underscoring the power of solvent engineering in directing complex cluster assembly. These high-nuclearity clusters demonstrated promising functionality in electrocatalytic CO_2 reduction, with the layered Sn_{26} cluster achieving a Faradaic efficiency of 41.9% for formate production[58].

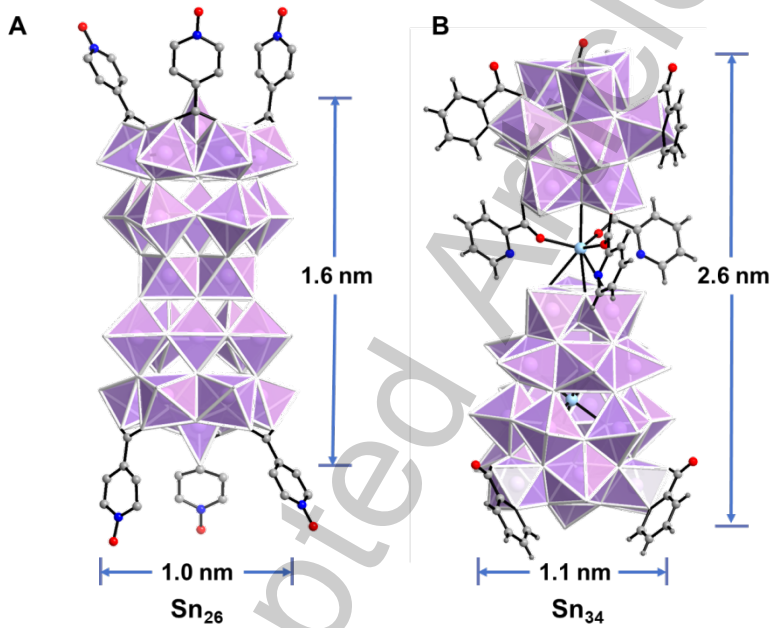

Figure 4. High-nuclearity architectures of rod-like Sn_{26} (A) and the cage-type dimeric Sn_{34} cluster (B). Color code: Sn, purple; O, red; C, grey; N, blue; Na, light blue. The crystal structures (A-B) were redrawn based on crystallographic data from literature[58], with permission from Royal Society of Chemistry.

The structural engineering of organotin-oxo clusters has advanced significantly, evolving from simple cage-like frameworks to complex macrocyclic architectures through deliberate ligand design and synthetic condition optimization, marking a strategic shift toward dimensional control and function integration. A pivotal example is the rational construction of a series of selenite-bridged organotin-oxo macrocycles - $[(n\text{-}BuSn)_8(SeO_3)_{16}]$ (macrocyclic Sn_8), $[(n\text{-}BuSn)_{12}(\mu_2\text{-}O)_4(\mu_3\text{-}O)_{12}(SeO_3)_8]$ (Sn_{12}-α), $[(n\text{-}BuSn)_{12}(ClO_4)(\mu_3\text{-}O)_{12}(SeO_3)_8]$ (Sn_{12}-β), and $[(n\text{-}BuSn)_{12}Fe_{18}(\mu_4\text{-}O)_6(C_2H_4O_2)_{24}(SeO_3)_{18}]$ ($Sn_{12}Fe_{18}$) - *via* selenite ligand-driven supramolecular assembly [**Figure 5**][59]. All

clusters are synthesized under solvothermal conditions, with the trigonal pyramidal geometry of selenite ligands (SeO_3^{2-}) and their versatile coordination modes serving as the key directing forces for cyclic architecture formation. Specifically, Sn_8 is prepared by reacting n-$BuSnCl_3$, SeO_2, and $MnCO_3$ in a methylamine/dimethyl sulfoxide (DMSO) mixed solvent; Sn_{12}-α and Sn_{12}-β crystallize in different space groups througu tailored solvothermal systems; and $Sn_{12}Fe_{18}$ is obtained by integrating Fe^{2+}/Fe^{3+} ions into the n-butyltin–selenite assembly system, forming the largest reported organotin macrocycle to date. Structurally, Sn_8 features an octanuclear crown-shaped ring with an outer diameter of ~1.5 nm, composed of 8 alternating n-butyltin units and 16 selenite ligands. Half of the selenite ligands bridge adjacent n-butyltin units on the outer rim, while the other half anchor to the inner rim. Each Sn center adopts a distorted octahedral {$BuSnO_5$} coordination environment, with n-butyltin units staggered above and below the ring plane to form a noncoplanar structure resembling S_8. Sn_{12}-α possesses a near-square macrocycle core {(n-BuSn)$_{12}O_{16}$}, constructed by four {Sn_3O_4} defective cubane fragments interconnected in a head-to-tail manner. The core is stabilized by 4 μ_2-O and 12 μ_3-O bridges, with 8 selenite ligands on the outer ring; Sn_{12}-β is derived from Sn_{12}-α by introducing a chloride ion into the central cavity *via* Cl-O bonds; and $Sn_{12}Fe_{18}$ (2.9 nm outer diameter) forms a heterobimetallic single-layer ring integrating a {Fe_{18}} framework linked to 12 n-butyltin units through EG and selenite bridges. This series exhibits exceptional electron-beam lithography (EBL) performance, with Sn_{12}-α achieving a high-resolution patterning capability of 50 nm at a low dose of 50 μC/cm^2, attributed to its optimal Sn/Se stoichiometry, compact molecular architecture, and homogeneous film-forming ability (surface roughness: 0.59 nm).

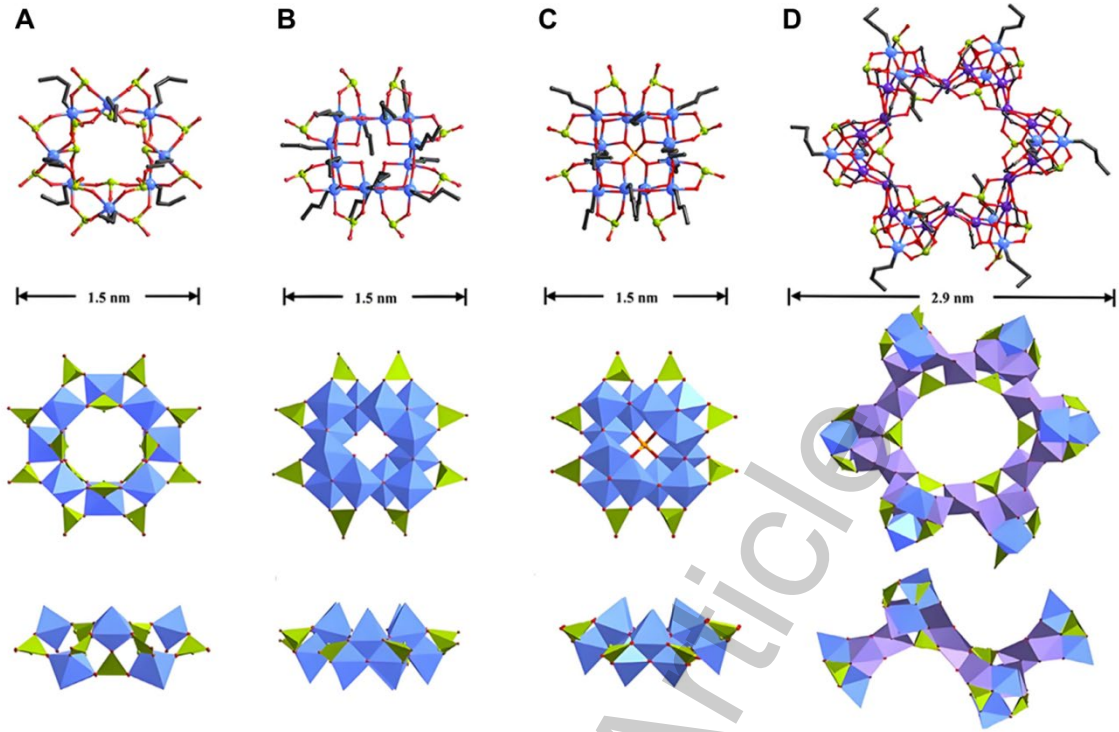

Figure 5. Ball-and-stick representations and corresponding polyhedral views of Sn_8 (A), Sn_{12}-α (B), Sn_{12}-β (C), and $Sn_{12}Fe_{18}$ (D), respectively. Color code: Sn, blue; O, red; C, black; Se, lime; Cl, orange; Fe, purple. (A-D)Reproduced with permission[59]. Copyright 2025, Wiley-VCH.

Non-alkyl TOCs

Current studies predominantly focus on alkyl-functionalized systems, while research on environmentally friendly non-alkyl TOCs remains very limited and is still in its early stages. The synthesis of non-alkyl tin-oxo clusters typically relies on the hydrolysis of inorganic tin salts [**Figure 6**]. However, the rapid and poorly controlled hydrolysis kinetics often lead to the precipitation of amorphous tin oxides or hydroxides, rather than discrete molecular clusters. Thus, the selection of suitable solvents and ligands to regulate the hydrolysis rate of inorganic tin precursors is crucial for the directed assembly of non-alkyl TOCs.

A pivotal methodological advance was reported in 2020 by Zhang et al., who introduced the "coordination-delayed hydrolysis" strategy by employing low-toxicity $SnCl_4 \cdot 5H_2O$ as a precursor in combination with a pyrazole (PZ) thermolysis approach[60]. In this system, PZ serve as dual-function ligands, where their N-donor coordination to Sn(IV)

centers kinetically delays the hydrolysis rate, while their hydrogen-bonding capability stabilizes the resulting cluster assembly. Notably, the low melting point of PZ (~66−70 °C) allows it to act as a reaction medium at the synthetic temperature (100 °C), defining the "pyrazole-thermal synthesis" that enables green and efficient preparation of non-alkyl TOCs. This approach successfully yielded a series of well-defined non-alkyl TOCs with precise nuclearity, including Sn_{10} cluster $[Sn_{10}(\mu_3\text{-}O)_8(\mu_2\text{-}O)_4(PZ)_8(HPZ)_4Cl_8)]$ and Sn_{14} cluster. The Sn_{10} cluster features a central $\{Sn_6\}$ octahedron connected to four peripheral Sn atoms *via* μ_3-O bridges, with the entire $\{Sn_{10}O_{12}\}$ core stabilized by 8 bridged PZ ligands, 4 mono-coordinated HPZ ligands, and 8 terminal Cl^- ions for charge balance. The Sn_{14} cluster extends the $\{Sn_{10}\}$ core by adding four extra peripheral Sn centers linked through μ_2-OH bridges. Remarkably, the strategy supports heterometallic extension. By introducing $Ti(OiPr)_4$ into the Sn_{10} reaction system, the team synthesized a bimetallic Sn_4Ti_6-oxo cluster $[Sn_4Ti_6(\mu_3\text{-}O)_8(\mu_2\text{-}O)_4(PZ)_8(HPZ)_4Cl_8]$, where the central $\{Sn_6\}$ octahedron is replaced by a $\{Ti_6\}$ octahedron. The Sn_{10} cluster achieved a maximum faradaic efficiency (FE) of ~57% for formate production at −1.0 V (*vs* reversible hydrogen electrode, RHE) in CO_2 reduction reactions (CO_2RR), significantly outperforming the classical alkyl-Sn_{12} cluster (~26% FE at −1.2 V vs RHE).

A recent study further advanced non-alkyl TOC design by introducing a reflux-based solution synthesis for scalable production of a novel cyclic non-alkyl cluster, $[Sn_4Cl_3(C_3N_2H_4)(C_3N_2H_3)H_4O_8]$[61]. Its EUV linear absorption coefficient reaches 20.7 μm^{-1}, higher than typical tin oxide-based resists (10–19.7 μm^{-1}), attributed to its high molecular EUV photoionization cross section and dense structure. In EBL, it achieves clear 40–50 nm half-pitch patterns at doses of 1500–2000 $\mu C/cm^2$. Under EUV lithography (EUVL), it forms 18–22 nm half-pitch patterns at 105 mJ/cm^2, with line edge roughness (LER) of ~3.7 nm and a critical dimension of 12.8 nm after hard baking.

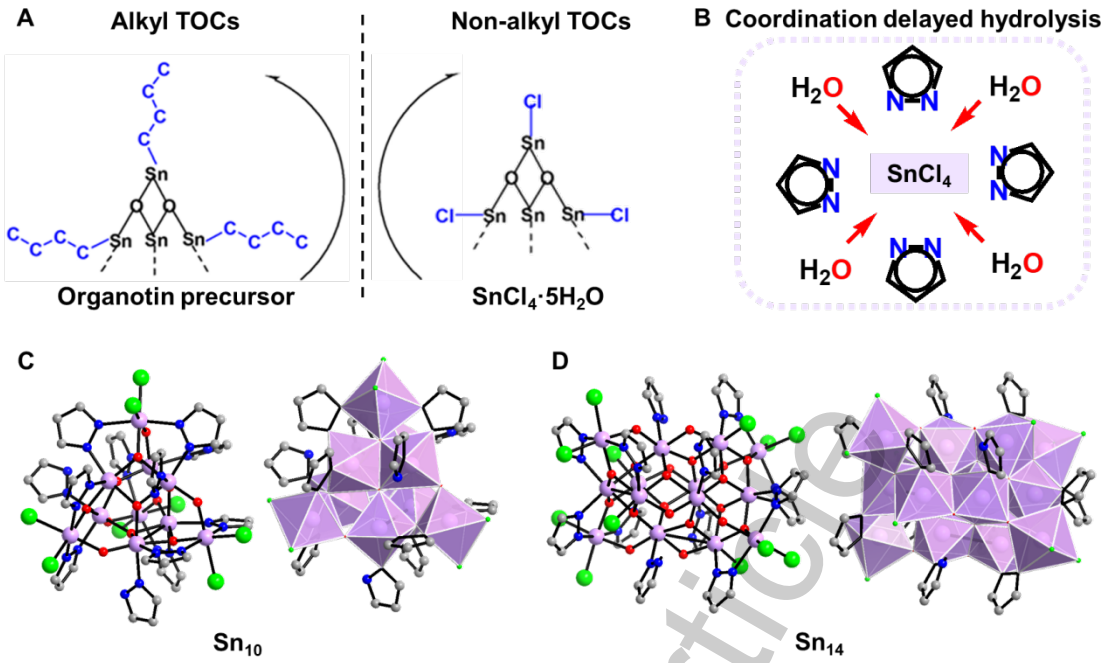

Figure 6. (A) Comparison between the alkyl TOCs using organotin precursor with stable Sn–C bonds and non-alkyl TOCs using inorganic tin salts. (B) Schematic illustration of the coordination delayed hydrolysis strategy. (C) Ball-and-stick and polyhedral views of Sn_{10}. (D) Ball-and-stick and polyhedral views of Sn_{14}. Color code: Sn, purple; O, red; N, blue; C, gray; Cl, green. (A-D) Reproduced with permission[60]. Copyright 2020, Chinese Chemical Society.

Heterometallic TOCs

Homometallic TOCs face inherent constraints that limit their structural diversity and tunability. The high stability of the Sn–C bonds, inherited from the organotin precursors, strongly directs the assembly process toward the formation of rigid, hollow Sn–O frameworks with limited architectural variety. This structural predictability, coupled with their compositional homogeneity and restricted electronic configurability, narrows the pathways for deliberate molecular design and functionalization. To overcome these limitations, the introduction of heterometallic centers has emerged as a powerful strategy in cluster chemistry. The incorporation of secondary metal ions disrupts the symmetric bonding environment dominated by Sn–C interactions, enabling access to previously inaccessible structural motifs. Furthermore, the distinct coordination geometries, oxidation states, and electronic configurations of the secondary metals provide enhanced control over the cluster's architecture and physical characteristics. These modifications

lead to improved light absorption, tunable band structures, and optimized charge-transfer properties, while also enabling more versatile ligand functionalization.

Heterometallic TOC synthesis leverages size matching (between Sn and secondary metal ions) and ligand compatibility (to coordinate both metals) to ensure structural integrity, with key advances in the incorporation of noble metal, rare-earth, and transition/main-group metal. Noble metals (Ag, Ru) introduce "heavy atom effects" and redox activity, making them useful for NLO and catalysis. Zhang and co-workers developed the first silver-templated γ-Keggin-type alkyl tin-oxo cluster, $[(n\text{-}BuSn)_{12}(OH)_{23}O(AgO_4)]_2 \cdot 6(Ac) \cdot 2(PCA) \cdot 7CH_3CN$ ($AgSn_{12}$), *via* strategic size and charge matching, where the central Ag^+ ion (radius ~115 pm) not only fits perfectly within the Keggin cavity but also introduces a heavy atom effect that induces additional symmetry-allowed electronic transitions [**Figure 7**]. Theoretical calculations reveal that both the Sn–O inorganic shell and the peripheral butyl groups contribute to the strong third-order NLO response. This unique electronic structure endows the $AgSn_{12}$ cluster with a strong third-order NLO response and excellent optical limiting performance, exhibiting a nonlinear absorption coefficient of 2.55×10^{-9} m/W and an optical limiting threshold as low as 0.502 J/cm^2[62]. Chandrasekhar et al. obtained ruthenium-derivatized "drum-type" tin-oxo clusters *via* reflux and slow evaporation techniques, specifically through the reaction of ruthenocene carboxylic acid (RcCOOH) with organotin precursors such as $[n\text{-}BuSn(O)OH]_n$, $(Ph_3Sn)_2O$, and $(PhCH_2)_3SnCl$. These clusters feature a prismane-like $\{Sn_6O_6\}$ core stabilized by six ruthenocene carboxylate ligands[63]. Lu et al. synthesized a novel $\{[Cl@Ag_{12}(tBu{\equiv}C)_6][(n\text{-}BuSn)_3(\mu_3\text{-}O)(tBuPO_3)_3(OMe)(OH)_2]_2\}(OH)$ cluster by reacting alkynyl silver ($tBuC{\equiv}CAg$) with butylstannonic acid in methanol, using $AgBF_4$ as an auxiliary metal source and Me_4NCl (indispensable for core stabilization) to introduce Cl^-. Structurally, the cluster has a central $[Cl@Ag_{12}(tBuC{\equiv}C)_6]^{5+}$ cationic core, six $tBuC{\equiv}C^-$ adopt μ_3-bridging) capped by two anionic $[(n\text{-}BuSn)_3(\mu_3\text{-}O)(tBuPO_3)_3(OMe)(OH)_2]^{2-}$ organooxotin clusters; the two moieties are linked via Ag–O_p bonds, with Sn atoms hexacoordinated and tert-butylphosphonate ligands adopting μ_4-bridging to consolidate the architecture[64].

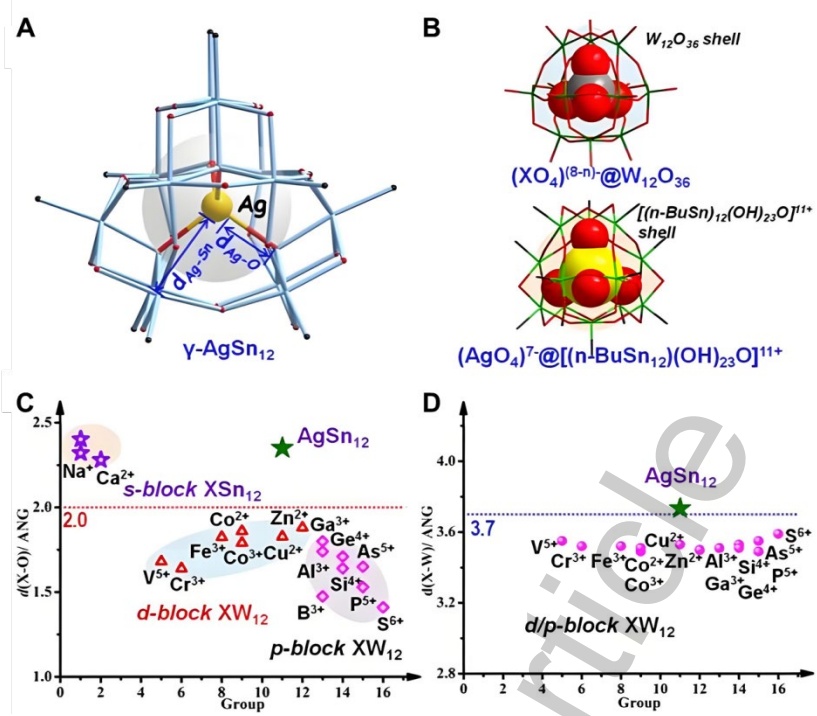

Figure 7. Structural and geometric analysis of the silver-templated tin Keggin cluster. (A) Ball-and-stick model of the $AgSn_{12}$ Keggin cluster. (B) Comparative structural models of the classic XW_{12} and the $AgSn_{12}$ Keggin clusters. (C) Comparison of the average X–O bond lengths in $AgSn_{12}$, XW_{12}, and XSn_{12} Keggin systems. (D) The average distances between the central heteroatom and the framework metals (X···W and Ag···Sn) in $AgSn_{12}$ and XW_{12} clusters. Color code: O, red; C, black; heteroatom (X), gray; Ag, yellow. (A-D)Reproduced with permission[62]. Copyright 2022, Wiley-VCH.

Rare-earth metals (such as Eu, Er, Ho) are ideal heterometallic centers for TOCs due to their well-defined oxidation states (RE^{3+}) and tunable ionic radii, enabling precise structural modulation and photoluminescent properties[65]. Through precise molecular design, Zhang et al. constructed $[(PhSn)_4Sn_2Eu_4(\mu_2\text{-}OH)_4(\mu_4\text{-}O)_6(GA)_4(DMF)_4(NE)_4]$ (Sn_6Eu_4, H_2GA = glycolic acid, H_2NE = *cis*-5-norbornene-endo-2,3-dicarboxylic acid) and $[(n\text{-}BuSn)_8Sn_4Eu_8(\mu_4\text{-}O)_{12}(GA)_8(HGA)_8(NE)_8]$ ($Sn_{12}Eu_8$) clusters using tetranuclear $\{Sn_2Eu_2\}$ building blocks. Sn_6Eu_4 features a heterometallic core with Sn atoms on the periphery and Eu atoms internally, assembled *via* vertex-/edge-sharing of $\{Sn_2Eu_2\}$ units, surrounded by GA, NE ligands, and terminal DMF molecules. $Sn_{12}Eu_8$ adopts an inter-cluster docking structure, formed by two ligand-bridged $\{Sn_6Eu_4\}$ moieties linked *via* GA ligands (each coordinating two Eu from one moiety and one Sn/Eu from the other), representing the largest heterometallic tin-lanthanide oxo cluster reported at the time.

When smaller Er ions were used, a distinct $[(n\text{-}BuSn)_{13}Er_6(\mu_2\text{-}O)_2(\mu_2\text{-}OH)_{13}(\mu_3\text{-}OH)_9(\mu_4\text{-}O)_6(NE)_9]Cl\cdot 6DMF$ ($Sn_{13}Er_6$) cluster with an asymmetric trigonal pyramidal configuration formed. The apex is a $\{Sn_4Er_3\}$ motif (assembled from three $\{Sn_2Er_2\}$ units *via* shared edges and a central Sn vertex), and the base consists of three inequivalent $\{Sn_3Er\}$ subunits, with each $\{Sn_3Er\}$ sharing one Er atom with the apex to complete the skeleton. This structural divergence highlights lanthanide ionic size as a critical structural determinant. Notably, the optimized $Sn_{13}Er_6$ cluster exhibits high solution stability (confirmed by ESI-MS with a dominant peak at m/z = 2724.8064 corresponding to its intact cationic form) and is stabilized by NE ligands with four unique coordination patterns that promote irradiation-induced crosslinking *via* alkenyl groups. It achieved 50 nm patterning at a low exposure dose of 50 $\mu C/cm^2$, and demonstrated remarkable sensitivity with lithographic reactions initiating at just 10 $\mu C/cm^2$, which can be attributed to the synergistic effect of the Sn-Er heterometallic core and functional NE ligands [66].

Transition metals (Ti, Fe, V, Zr) and main-group metals (In, Al, Ga) introduce diverse coordination geometries and redox activity, enabling TOCs to address specific application needs. For example, the introduction of Ti leads to the formation of an undecametric $\{Sn_6Ti_5\}$ core in $[(n\text{-}BuSn)_6Ti_5(\mu_3\text{-}O)_{10}(OMe)_2(L_1)_8]$ (SnTi-1, H_2L_1 = salicylaldoxime) and $[(n\text{-}BuSn)_6Ti_5(\mu_3\text{-}O)_{10}(OMe)_2(L_2)_8]\cdot 4(MeOH)$ (SnTi-2, H_2L_2 = o-vanillaldoxime), where a pentagonal Ti_5 wheel is fused with two Sn_3 trimers. The subtle substitution from salicylaldoxime to o-vanillaldoxime alters the intermolecular interactions from C–H···π to π···π stacking, which effectively modulates the third-order NLO behavior from saturable absorption ($\beta = -0.24\times10^{-10}$ m/W) to reverse saturable absorption ($\beta = +0.4\times10^{-10}$ m/W), demonstrating precise control over optical switching and limiting capabilities[67]. Similarly, the incorporation of Ga^{3+} and Mn^{2+} into a selenite-based framework in $[(BuSn)_4Ga_2Mn_2O_6(SeO_3)_6]$ creates a discrete trimetallic cluster that combines photocurrent conversion with ferromagnetic behavior, showcasing the power of heterometal integration to embed multiple physical properties within a single molecular entity[68]. A series of isostructural dumbbell-type clusters, $[(n\text{-}BuSn)_{12}In_2(\mu_4\text{-}O)_2(CH_3O)_8(C_6H_5PO_3)_6(CH_3OH)_2]$ (SnOC-1(In)), along with its iron and aluminum analogues $[(n\text{-}BuSn)_6Fe_2(\mu_3\text{-}O)_2(CH_3O)_8(C_6H_5PO_3)_6(CH_3OH)_2]$ (SnOC-1(Fe)) and $[(n\text{-}BuSn)_6Al_2(\mu_3\text{-}O)_2(CH_3O)_8(C_6H_5PO_3)_6]$ (SnOC-1(Al)), demonstrates the efficacy of

introducing heterometallic centers for coordination-driven structural diversification [**Figure 8**][69]. These {M_2Sn_6} clusters share a common architecture where two {(n-BuSn)$_3$(μ_3-O)} triangular units are linked *via* phenylphosphonate bridges to a central heterometal-oxo unit. Despite their similar overall topology, the local coordination geometry of the secondary metal ions varies significantly, ranging from octahedral (In, Fe) to trigonal bipyramidal (Al). This geometric difference, particularly the unsaturated coordination of the Al^{3+} center, directly influences cluster stability and was found to be a key factor in enhancing lithographic sensitivity, thereby highlighting the critical role of coordination unsaturation in patterning performance.

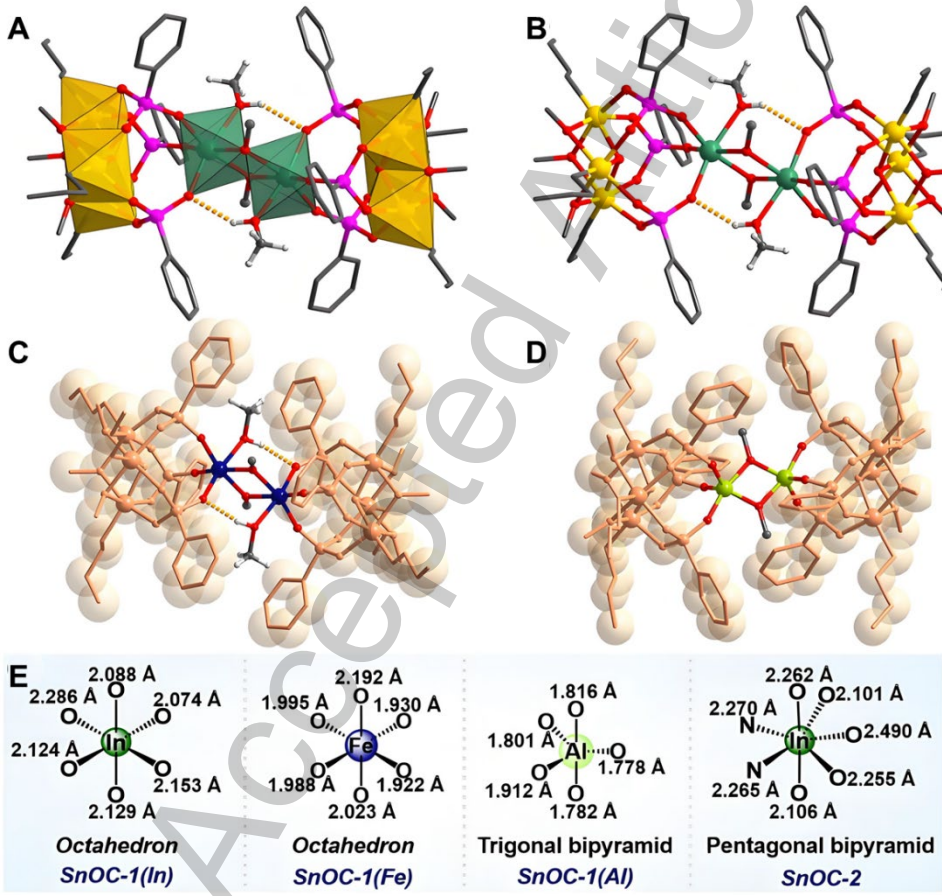

Figure 8. (A, B) Molecular structure of SnOC-1(In) depicted in polyhedral and ball-and-stick representations, respectively. (C, D) Molecular structures of SnOC-1(Fe) and SnOC-1(Al). (E) The coordination environments of the heterometallic centers in the clusters. Color code: Sn, gold; In, sea green; Fe, navy; Al, lime green; O, red; C, grey. Polyhedra: {SnO_5C}, gold; {InO_6}, sea green. (A-E)Reproduced with permission[69]. Copyright 2025, Wiley-VCH.

The incorporation of vanadium enabled the construction of the first well-defined heterometallic tin-vanadium oxo cluster, $[(n\text{-}BuSn)_8V_2O_8(OH)_4(TEA)_2(L)_6]$ (TEA = triethanolamine)[70]. Synthesized through a one-pot solvothermal reaction (80 °C, 72 h) of butyltin oxide, vanadium(IV)oxy acetylacetonate, and carboxylate ligands in acetonitrile (with triethanolamine/triethylamine as additives), the cluster features a robust $\{Sn_8V_2\}$ core assembled from two $\{Sn_4V(TEA)(L)_3\}$ subunits linked by shared oxygen atoms. Structurally, the four Sn centers exhibit diverse coordination environments: Sn1 adopts a rare pentagonal bipyramidal $\{SnO_7\}$ geometry, while Sn2–Sn4 form octahedral $\{SnO_5C\}$ moieties (each bonded to a butyl group), and two V^{4+} centers adopt distorted octahedral configurations. Vanadium centers effectively disrupts the closed coordination environment imposed by Sn–C bonds, creating six accessible functionalization sites on the cluster surface. These sites enable precise modification with 12 different carboxylate ligands (including olefin-containing, halogen-substituted, and cyclopropyl ligands) and the controlled synthesis of 10 hybrid mixed-ligand clusters (e.g., *via* competitive ligand coordination. Crystallographic monitoring and DFT calculations reveal the assembly mechanism: initial formation of the $\{Sn_8V_2\}$ core with surface hydroxyl groups, followed by dehydration condensation with carboxylate ligands, and dynamic ligand exchange in mixed-ligand systems. This breakthrough establishes an ideal molecular platform for systematically regulating lithographic performance. EBL studies on these ligand-functionalized clusters revealed significant structure-activity relationships. Clusters modified with olefin-containing ligands exhibited higher lithographic sensitivity (450–990 μC/cm^2) than those with halogen or cyclopropyl ligands. This is attributed to the promotion of radical polymerization by C=C bonds and the electron-rich phenyl ring, which enhance cross-linking efficiency in exposed regions. The best-performing Sn_8V_2-L_1 (functionalized with *p*-vinylbenzoic acid) achieved 30 nm line/space resolution at 200 μC/cm^2. This ligand variation-driven EBL optimization provides a reliable screening approach for developing high-performance resists - an essential link between synthetic innovation and practical application of TOCs.

In a recent study, the heterometallic strategy was further exemplified by the solvothermal synthesis of the first heterometallic Zr-Sn-oxo clusters. Using a heart-shaped (Zr_6-oxo) octahedron as a core template, four peripheral organotin units are integrated to form a series of Zr_6Sn_4-oxo clusters with the general formula $[(n\text{-}BuSn)_4Zr_6Cl_2(\mu_3\text{-}O)_4(\mu_4\text{-}$

O)$_4$(μ-MeO)$_8$L$_{10}$], where L denotes different halogenated benzoate ligands [**Figure 9**]. The resulting architecture features a {Zr$_6$} octahedron encapsulated within a larger {Sn$_4$} tetrahedron, constituting a unique nested geometry. The cluster periphery is further stabilized and functionalized by ten halogenated benzoate ligands, which exhibit remarkable coordination flexibility by adopting bidentate modes to bridge either Zr–Zr, Zr–Sn, or Zr–(Sn–Cl) pairs. For the synthesis, n-butyltin oxide (n-BuSnOOH) was used as the organotin precursor, $ZrOCl_2 \cdot 8H_2O$ as the Zr source, and various halogenated benzoic acids (p-chlorobenzoic acid, p-fluorobenzoic acid, m-trifluoromethylbenzoic acid) as ligands. The reactants were sealed in 20 mL vials with mixed solvent systems and the mixed solvents were tailored to each ligand to optimize solubility and crystal growth conditions. The m-trifluoromethylbenzoate-decorated cluster demonstrated exceptional lithographic sensitivity, achieving 50 nm line patterns at exposure dose of 50 μC/cm^2[71].

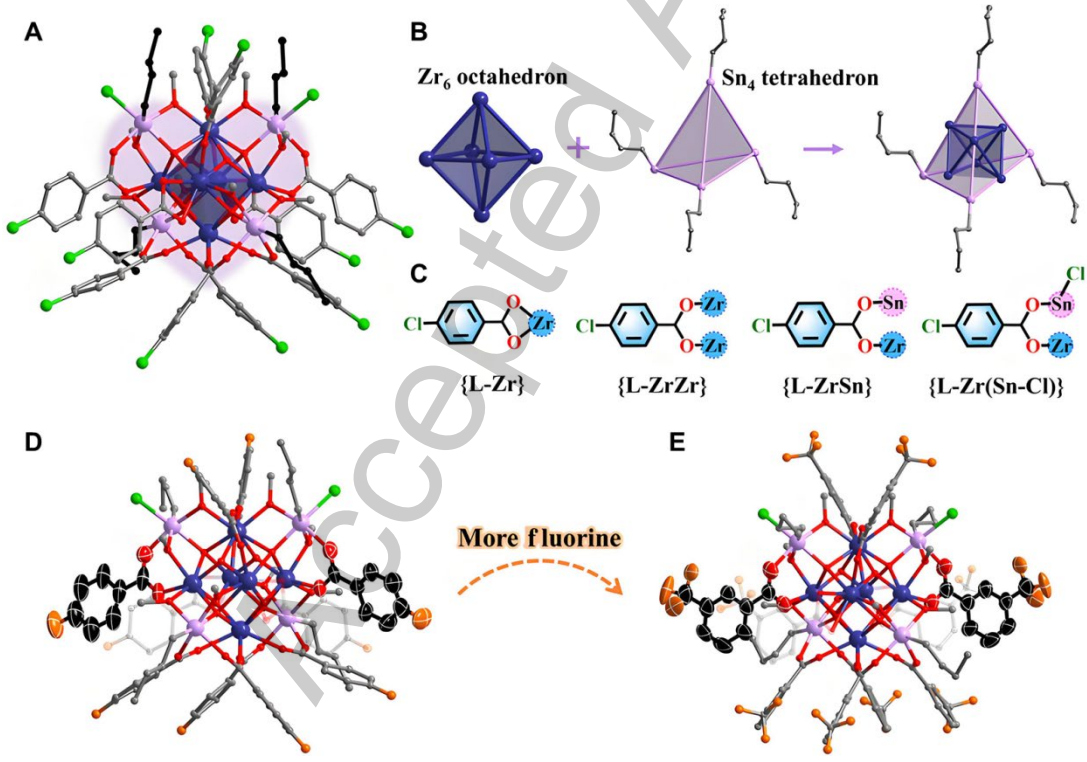

Figure 9. (A) Molecular structure of the Zr$_6$Sn$_4$-oxo cluster functionalized with p-chlorobenzoate ligands. (B) Schematic illustration of the core assembly in the Zr$_6$Sn$_4$ cluster. (C) Coordination modes of the p-chlorobenzoate ligands. (D, E) Molecular structures of the p-fluorobenzoate-decorated Zr$_6$Sn$_4$ cluster and the m-trifluoromethylbenzoate-decorated cluster, respectively. Color code: Zr, dark blue; Sn,

purple; Cl, green, F, orange; O, red; C, gray. (A-E)Reproduced with permission[71]. Copyright 2025, Chinese Chemical Society.

CONCLUSION AND OUTLOOK

In conclusion, TOCs have emerged as a versatile class of molecular materials with precisely tunable structures and multifunctional properties. Through advanced synthetic strategies such as ligand-directed assembly and heterometallic incorporation, a diverse range of architectures have been constructed. These structurally well-defined clusters not only provide atomic-level insight into the coordination behavior and reactivity of tin oxides but also demonstrate remarkable functional performance, particularly in areas including high-resolution nanolithography, tunable NLO properties, and electrocatalysis, highlighting their potential as functional molecular platforms.

Looking ahead, the field faces the critical challenge of shifting from exploratory synthesis to predictive molecular design. Future research could focus on the development of quantitative structure-property relationships, supported by computational guidance and *in situ* mechanistic studies, to enable precision engineering of TOCs for application-specific requirements. Emphasis on environmentally benign non-alkyl TOCs and sustainable synthesis pathways will further align material development with green chemistry principles. Moreover, successful integration of TOCs into functional devices will demand innovative solutions to interfacial assembly, morphological control, and operational stability under realistic conditions. By addressing these challenges through interdisciplinary collaboration, TOCs are poised to play an expanding role in next-generation nanotechnologies, energy conversion systems, and advanced photonic devices.

DECLARATIONS

Authors' contributions

Conducted the literature survey and wrote the initial draft: Zhen N;

Provided critical feedback, revised the manuscript: Liu FF, Zhou ZH, Zhang L;

Supervised the project and secured funding: Zhang L.

Availability of data and materials

Not applicable.

Financial support and sponsorship

This work is supported by National Natural Science Foundation of China (22271284 and 92461315), the Fundamental Research Funds for the Central Universities, Nankai University (075-63243140), and Young Scientific and Technological Talents (Level One) in Tianjin.

Conflicts of interest

All authors declared that there are no conflicts of interest.

Ethical approval and consent to participate

Not applicable.

Consent for publication

Not applicable.

REFERENCES

1. Long DL, Tsunashima R, Cronin L. Polyoxometalates: Building blocks for functional nanoscale systems. *Angew Chem Int Ed* 2010;49:1736-1758. DOI: 10.1002/chin.201018216

2. López X, Carbó J, Bo C, et al. Structure, properties and reactivity of polyoxometalates: a theoretical perspective. *Chem Soc Rev* 2012;41:7537-7571. DOI: 10.1039/C2CS35168D

3. Nyman M, Burns PC. A comprehensive comparison of transition-metal and actinyl polyoxometalates. *Chem Soc Rev* 2012;41:7354-7367. DOI: 10.1039/c2cs35136f

4. Dolbecq A, Dumas E, Mayer CR, et al. Hybrid organic-inorganic polyoxometalate compounds: From structural diversity to applications. *Chem Rev* 2010;110:6009-6048. DOI: 10.1021/cr1000578

5. Eynden DV, Pokratath R, Roo JD. Nonaqueous chemistry of group 4 oxo clusters and colloidal metal oxide nanocrystals. *Chem Rev* 2022;122:10538-10572. DOI: 10.1021/acs.chemrev.1c01008

6. Wang SS, Yang GY. Recent advances in polyoxometalate-catalyzed reactions. *Chem Rev* 2015;115:4893-4962. DOI: 10.1021/cr500390v

7. Kalandia G, Declerck K, Salazar Marcano DE, et al. Finding the key: Binding of metal-oxo clusters to the enzyme active site enabled by "click" (bio)conjugation. *Angew Chem Int Ed* 2025;64:e202518349. DOI: 10.1002/anie.202518349

8. Mialane P, Mellot-Draznieks C, Gairola P, et al. Heterogenisation of polyoxometalates and other metal-based complexes in metal–organic frameworks: from synthesis to characterisation and applications in catalysis. *Chem Soc Rev* 2021;50:6152-6220. DOI: 10.1039/d0cs00323a

9. Miras HN, Yan J, Long DL, et al. Engineering polyoxometalates with emergent properties. *Chem Soc Rev* 2012;41:7403-7430. DOI: 10.1039/c2cs35190k

10. Guo L, He L, Zhuang Q, et al. Recent advances in confining polyoxometalates and the applications. *Small* 2023;19:e2207315. DOI: 10.1002/smll.202207315

11. Fay B. Advanced optical lithography development, from UV to EUV. *Microelectro Eng* 2002;61-61:11-24. DOI: 10.1016/S0167-9317(02)00427-6

12. Yeh CC, Liu HC, Heni W, et al. Chemical and structural investigation of zinc-oxo cluster photoresists for DUV lithography. *J. Mater. Chem. C* 2017;5:2611-2619. DOI: 10.1039/c6tc05201k

13. Thakur N, Bliem R, Mochi I, et al. Mixed-ligand zinc-oxoclusters: efficient chemistry for high resolution nanolithography. *J. Mater. Chem. C* 2020;8:14499-14506. DOI: 10.1039/d0tc03597a

14. Wu LJ, Bespalov I, Witte K, et al. Unravelling the effect of fluorinated ligands in hybrid EUV photoresists by X-ray spectroscopy. *J. Mater. Chem. C* 2020;8:14757-14765. DOI: 10.1039/D0TC03216F

15. Wang Q, Cui H, Wang X, et al. Exceptional light sensitivity by thiol-ene click lithography. *J Am Chem Soc* 2023;145:3064-3074. DOI: 10.1021/jacs.2c11887

16. Zhang M, Yang S, Liu M, et al. Tungstotellurate(VI)-based nanocomposite inhibits breast cancer proliferation and metastasis by enhancing cuproptosis and apoptosis. *Angew Chem Int Ed* 2025;e202514795. DOI:10.1002/anie.202514795

17. Rhule JT, Hill CL, Judd DA. Polyoxometalates in medicine. *Chem Rev* 1998;98:327-357. DOI: 10.1021/cr960396q

18. Li B, Xu X, Lv Y, et al. Polyoxometalates as potential artificial enzymes toward biological applications. *Small* 2023;20:2305539. DOI: 10.1002/smll.202305539

19. Čolović MB, Lacković M, Lalatović J, et al. Polyoxometalates in biomedicine: Update and overview. *Curr Med Chem* 2020;27:362-379. DOI: 10.2174/0929867326666190827153532

20. Yi X, Fang W, Liu J, et al. Structural chemistry of metal-oxo clusters. *WILEY-VCH* 2021.

21. Gumerova NI, Rompel A. Polyoxometalates in solution: speciation under spotlight. *Chem Soc Rev* 2020;49:7568-7601. DOI: 10.1039/D0CS00392A

22. Zhang D, Wang C, Lin Z, et al. Fullerene-like niobovanadate cage built from {(Nb)V_5} pentagon. *Angew Chem Int Ed* 2024;63:e202320036. DOI: 10.1002/anie.202320036

23. Lin J, Li N, Yang S, et al. Self-assembly of giant Mo_{240} hollow opening dodecahedra. *J Am Chem Soc* 2020;142:13982-13988. DOI: 10.1021/jacs.0c06582

24. Li Z, Li XX, Yang T, et al. Four-shell polyoxometalates featuring high-nuclearity Ln_{26} clusters: structural transformations of nanoclusters into frameworks triggered by transition-metal ions. *Angew Chem Int Ed* 2017;56:2664-2669. DOI: 10.1002/anie.201612046

25. Sadeghi O, Amiri M, Reinheimer EW, et al. The role of Bi^{3+} in promoting and stabilizing iron oxo clusters in strong acid. *Angew Chem Int Ed* 2018;57:6247-6250. DOI: 10.1002/anie.201802915

26. Gao M-Y, Wang Z, Li Q-H, et al. Black titanium-oxo clusters with ultralow band gaps and enhanced nonlinear optical performance. *J Am Chem Soc* 2022;144:8153-8161. DOI: 10.1021/jacs.2c00765

27. Fan X, Yuan F, Li D, et al. Threefold collaborative stabilization of Ag_{14}-nanorods by hydrophobic Ti_{16}-oxo clusters and alkynes: Designable assembly and solid-state optical-limiting application. *Angew Chem Int Ed* 2021;60:12949-12954. DOI: 10.1002/anie.202101664

28. Liu YJ, Li QH, Li DJ, et al. Designable Al_{32}-oxo clusters with hydrotalcite-like structures: Snapshots of boundary hydrolysis and optical limiting. *Angew Chem Int Ed* 2021;60:4849-4854. DOI: 10.1002/anie.202012919

29. Maeno Z, Yasumura S, Liu C, et al. Experimental and theoretical study of multinuclear indium-oxo clusters in CHA zeolite for CH_4 activation at room temperature. *Phys Chem Chem Phys* 2019;21:13415-13427. DOI: 10.1039/c9cp01873e

30. Schubert U. Structures of large tin(IV) oxo clusters. *Z Anorg Allg Chem* 2024;650:e202400058. DOI: 10.1002/zaac.202400058

31. Mansfeld D, Miersch L, Rüffer T, et al. From {$Bi_{22}O_{26}$} to chiral ligand-protected

{$Bi_{38}O_{45}$}-based bismuth oxido clusters. *Chem Eur J* 2011;17:14805-14810. DOI: 10.1002/chem.201102437

32. V C, K G, P T. Nanodimensional organostannoxane molecular assemblies. *Acc Chem Res* 2007;40:420-434. DOI: 10.1021/ar600061f

33. Zheng GL, Ma JF, Su ZM, et al. A mixed-valence tin-oxygen cluster containing six peripheral ferrocene units. *Angew Chem Int Ed* 2004;43:2409-2411. DOI: 10.1002/anie.200353359

34. Chandrasekhar V, Baskar V, Vittal JJ. A new structural form of tin in a double O-capped cluster. *J Am Chem Soc* 2003;125:2392-2393. DOI: 10.1021/ja0287478

35. Reuter H. Inclusion of metal ions within a tin-oxygen cage stabilized by organic residues: crystal structure of $[(iPrSn)_{12}O_4(OH)_{24}][Ag_7I_{11}]\cdot NaCl\cdot H_2O\cdot 10DMSO$. *Angew Chem Int Ed* 1991;32:1482-1484. DOI: 10.1002/anie.199114821

36. Cardineau B, Del Re R, Marnell M, et al. Photolithographic properties of tin-oxo clusters using extreme ultraviolet light (13.5 nm). *Microelectron Eng* 2014;127:44-50. DOI: 10.1016/j.mee.2014.04.024

37. Zhang Y, Haitjema J, Liu X, et al. Photochemical conversion of tin-oxo cage compounds studied using hard X-ray photoelectron spectroscopy. *J. Micro. Nanolithography, MEMS, MOEMS* 2017;16:023510. DOI: 10.1117/1.Jmm.16.2.023510

38. Brouwer AM, Ekinci Y, Kazazis D, et al. Extreme ultraviolet patterning of tin-oxo cages. *J. Micro. Nanolithography, MEMS, MOEMS* 2017;16:033510-033516. DOI: 10.1117/1.Jmm.16.3.033510

39. Frederick RT, Diulus JT, Hutchison DC, et al. Effect of oxygen on thermal and radiation-induced chemistries in a model organotin photoresist. *ACS Appl. Mater. Interfaces* 2019;11:4514-4522. DOI: 10.1021/acsami.8b16048

40. Haitjema J, Wu L, Giuliani A, et al. UV and VUV-induced fragmentation of tin-oxo cage ions. *Phys Chem Chem Phys* 2021;23:20909-20918. DOI: 10.1039/d1cp03148a

41. Tian XJ, Yu YZ, Lu Q, et al. Organic-inorganic high-valence Sn_{18}-oxo clusters: Direct utilization of an inorganic Sn(IV) source to improve the nuclearity and electrocatalytic CO_2 reduction properties. *Inorg Chem* 2022;61:6037-6044. DOI: 10.1021/acs.inorgchem.2c00038

42. Jiang Q, Zhang X, You J. SnO_2: A wonderful electron transport layer for perovskite solar cells. *Small* 2018;14:e1801154. 10.1002/smll.201801154

43. Deng HX, Li SS, Li J. Quantum confinement effects and electronic properties of

SnO_2 quantum wires and dots. *J. Phys. Chem. C* 2010;114:4841-4845. DOI: 10.1021/jp911035z

44. Lim G, Lee K, Choi S, et al. Organometallic and coordinative photoresist materials for EUV lithography and related photolytic mechanisms. *Coord Chem Rev* 2023;493:215307-215319. DOI: 10.1016/j.ccr.2023.215307

45. Ober CK, Kafer F, Yuan C. Recent developments in photoresists for extreme-ultraviolet lithography. *Polymer* 2023;280:126020. DOI: 10.1016/j.polymer.2023.126020

46. Luo C, Xu C, Lv L, et al. Review of recent advances in inorganic photoresists. *RSC Adv.* 2020;10:8385-8395. DOI: 10.1039/c9ra08977b

47. Holmes RR, Swamy KCK, Schmid CG, et al. Organotin clusters. 4. Cubic, butterfly, and oxygen-capped clusters of n-butyloxotin phosphinates. A new class of organotin compounds. *J Am Chem Soc* 1988;110:7060-7066. DOI: 10.1021/ja00229a019

48. Swamy KCK, Day RO, Holmes RR. A new structural form of tin in a cubic cluster. *J Am Chem Soc* 1987;109:5546-5548. DOI: 10.1021/ja00252a053

49. Carlos CC, Esparza-Ruiz A, Peña-Hueso A, et al. Organometallic tin compounds derived from 2-benzimidazole propionic acid. *Z Anorg Allg Chem* 2013;639:1122-1128. DOI: 10.1002/zaac.201300108

50. Li QL, Wang F, Zhang RF, et al. Syntheses and characterization of organostannoxanes derived from 2-chloroisonicotinic acid: Tetranuclear and hexanuclear. *Polyhedron* 2015;85:361-368. DOI: 10.1016/j.poly.2014.08.039

51. Holmes RR, Schmid CG, Chandrasekhar V, et al. Oxo carboxylate tin ladder clusters. A new structural class of organotin compounds. *J Am Chem Soc* 1987;109:1408-1414. DOI: 10.1021/ja00239a022

52. Chandrasekhar V, Schmid CG, Burton SD, et al. New drum and ladder organooxotin carboxylates. *Inorg Chem* 1987;26:1050-1056. DOI: 10.1021/ic00254a017

53. Dakternieks D, Zhu HJ, Tiekink ERT, et al. Synthesis, structure and reactions of $[(BuSn)_{12}O_{14}(OH)_6]Cl_2 \cdot 2H_2O$: solution studies using ^{119}Sn NMR and electrospray mass spectrometry. *J Organomet Chem* 1994;476:33-40. DOI: 10.1016/0022-328X(94)84137-3

54. Banse F, Ribot F, P. Toledano, et al. Hydrolysis of monobutyltin trialkoxides: Synthesis and characterizations of $\{(BuSn)_{12}O_{14}(OH)_6\}(OH)_2$. *Inorg Chem* 1995;34:6371-6379. DOI: 10.1021/ic00129a023

55. Hutchison DC, Stern RD, Zakharov LN, et al. Butyltin Keggin ion with a rare four-

coordinate Ca center. *Inorg Chem* 2020;59:2900-2909. DOI: 10.1021/acs.inorgchem.9b03261

56. Saha S, Park D-H, Hutchison DC, et al. Alkyltin Keggin clusters templated by sodium. *Angew Chem Int Ed* 2017;56:10140-10144. DOI: 10.1002/ange.201701703

57. Hutchison DC, Stern RD, Olsen MR, et al. Alkyltin clusters: the less symmetric Keggin isomers. *Dalton Trans* 2018;47:9804-9813. DOI: 10.1039/c8dt01950a

58. Zhu Y, Zhang L, Zhang J. Assembly of high-nuclearity Sn_{26}, Sn_{34}-oxo clusters: solvent strategies and inorganic Sn incorporation. *Chem Sci* 2019;10:9125-9129. DOI: 10.1039/c9sc02503k

59. Wang J, Luo MB, Wei ZJ, et al. Selenite-directed organotin-oxo macrocycles for nanolithography. *Angew Chem Int Ed* 2025;64:e202508220. DOI: 10.1002/anie.202508220

60. Wang D, Chen ZN, Ding QR, et al. Rational preparation of atomically precise non-alkyl tin-oxo clusters with theoretical to experimental insights into electrocatalytic CO_2 reduction applications. *CCS Chem* 2021;3:2607-2616. DOI: 10.31635/ccschem.020.202000546

61. Yun H, Heo S, Bang J, et al. Synthesis and characterizations of a nonalkyl tin oxo cluster and its application as high EUV absorption coefficient and etch resistant inorganic resist for EUV lithography. *Inorg Chem* 2025;64:5302-5321. DOI: 10.1021/acs.inorgchem.5c00495

62. Zhu Y, Wang ZR, Li DJ, et al. Silver-templated γ-Keggin alkyltin-oxo cluster: Electronic structure and optical limiting effect. *Angew Chem Int Ed* 2022;61:e202202853. DOI: 10.1002/anie.202202853

63. Kundu S, Chakraborty A, Mondal K, et al. Multi-ruthenocene assemblies on an organostannoxane platform. Supramolecular signatures and conversion to (Ru-Sn)O_2. *Cryst Growth Des* 2014;14:861-870. DOI: 10.1021/cg4017323

64. Junling J, Yun-Peng X, Xing L. High-nuclearity silver ethynide clusters containing polynucleating oxygen donor ligands. *Dalton Trans* 2018;47:12972-12978. DOI: 10.1039/C8DT02700E

65. Chen LJ, Hou Q, Cheng YJ, et al. Lanthanum-centered organotin oxysulfide clusters with substitutable coordinating amide solvent molecules for tuning blue light emission. *Cryst Growth Des* 2023;23:3098-3103. DOI: 10.1021/acs.cgd.3c00208

66. Liu FF, Wang D, Chen GH, et al. Alkenyl-type ligands functionalized tin-lanthanide

oxo nanoclusters as molecular lithography resists. *Sci China Chem* 2023;66:1731-1736. DOI: 10.1007/s11426-023-1598-3

67. Wang J, Luo M, Lin Q. Tuning third-order nonlinear optical response of heterometallic alkyltin-oxo clusters through intermolecular interactions. *J Solid State Chem* 2024;335:124723. DOI: 10.1016/j.jssc.2024.124723

68. Wei Z, Zhou X, Lin Q. Synthesis, photoluminescence and magnetism of a trimetallic selenide cluster: $(BuSn)_4Ga_2Mn_2O_6(SeO_3)_6$. *Inorg Chim Acta* 2022;535:120861. DOI: 10.1016/j.ica.2022.120861

69. Chen WZ, Wang LM, Wang ZR, et al. Improving the lithography sensitivity of atomically precise tin-oxo nanoclusters via heterometal strategy. *Angew Chem Int Ed* 2025;64:e202414360. DOI: 10.1002/anie.202414360

70. Zhen N, Zhou Z-H, Liu F-F, et al. Opening the coordination sphere of organotin oxo clusters through vanadium doping: From precise ligands engineering to tunable lithography reactivity. *CCS Chem* 2025;1-10. DOI: 10.31635/ccschem.025.202505929

71. Ye Y, Chen J, Chen W, et al. Synthesis, characterization, and radiation chemistry of fluorine-rich Zr-Sn-oxo clusters. *CCS Chem* 2025;1-11. DOI: 10.31635/ccschem.025.202405308